Carbon Nanotubes Activate Store-Operated Calcium Entry in Human Blood Platelets

Silvia H. De Paoli Lacerda,[†] Jana Semberova,[†,⊥] Karel Holada,[‡] Olga Simakova,[§] Steven D. Hudson,[¶] and Jan Simak[†,*]

[†]Center for Biologics Evaluation and Research, Food and Drug Administration, Rockville, Maryland 20852-1448, United States, [‡]1st Faculty of Medicine and [⊥]3rd Faculty of Medicine, Charles University, Prague, Czech Republic, [§]National Institutes of Health, Clinical Center, Bethesda, Maryland 20892, United States, and, [¶]National Institute of Standards and Technology, Gaithersburg, Maryland 20899, United States

Blood platelets are anucleated cells that originate from the bone marrow megakaryocytes and circulate in the blood as sentinels for vascular integrity. Platelets play a vital role in hemostasis; however, derangement of their functions can lead to thrombosis, which is a leading cause of death and disability in the developed world.[1] In view of the rapid development of nanotechnology, the impact of the newly engineered nanomaterials as an additional thrombosis risk factor is not yet known but should not be underestimated. In fact, it has been shown that inhaled carbon nanotubes (CNTs), one of the key building blocks in nanotechnology, are able to cross the epithelial barrier[2] to reach the circulation and cause thrombus formation.[3,4] Owing to their remarkable physical and chemical properties, CNTs hold a great promise for applications in several fields, including nanomedicine.[5] The industrial production of CNTs is increasingly raising concerns regarding the effects of environmental and work-related exposure. Moreover, CNTs are released in the atmosphere during the combustion of wood or clean-burning gas sources or from diesel engine.[6] In biomedical applications, CNTs are under development for use in diagnostic biosensors, drug delivery nanosystems, imaging nanoprobes for intravascular use and other devices that come in contact with blood.[7] Therefore, the assessment of the effect of CNTs in blood is a critical safety issue.

We have shown previously that different multiwalled CNTs (MWCNTs), but not fullerene (nC60), induce the aggregation of blood platelets;[8] MWCNTs activated platelets by inducing an influx of extracellular Ca^{2+}, an event that was sensitive to Ca^{2+} entry inhibitors. Here, we utilized immunofluorescence,

ABSTRACT Carbon nanotubes (CNTs) are known to potentiate arterial thrombosis in animal models, which raises serious safety issues concerning environmental or occupational exposure to CNTs and their use in various biomedical applications. We have shown previously that different CNTs, but not fullerene (nC60), induce the aggregation of human blood platelets. To date, however, a mechanism of potentially thrombogenic CNT-induced platelet activation has not been elucidated. Here we show that pristine multiwalled CNTs (MWCNTs) penetrate platelet plasma membrane without any discernible damage but interact with the dense tubular system (DTS) causing depletion of platelet intracellular Ca^{2+} stores. This process is accompanied by the clustering of stromal interaction molecule 1 (STIM1) colocalized with Orai1, indicating the activation of store-operated Ca^{2+} entry (SOCE). Our findings reveal the molecular mechanism of CNT-induced platelet activation which is critical in the evaluation of the biocompatibility of carbon nanomaterials with blood.

KEYWORDS: platelet activation · intracellular calcium · carbon nanotubes · fullerene · nanotoxicity · thrombosis

gold immuno-electron microscopy, and intracellular Ca^{2+} measurements to study the interaction between CNTs and platelets and the molecular mechanism of CNT-induced platelet activation. We demonstrate that MWCNTs induced extracellular Ca^{2+} influx in platelets by activation of the store-operated Ca^{2+} entry (SOCE). Therefore the CNT-induced platelet activation involves alterations in intracellular Ca^{2+}-homeostasis in platelets; this process occurs through modulation of tightly regulated Ca^{2+} channel rather than loss of plasma membrane integrity caused by perforation by CNTs.

RESULTS AND DISCUSSION

Carbon Nanoparticle (CNP) Characterization. To investigate a mechanism of CNT-induced platelet activation, we selected pristine MWCNTs with an average diameter of 60 nm (M60) from SES Research due to their relatively high purity, as determined by inductively coupled plasma mass spectrometry

© 2011 American Chemical Society

(ICP—MS) and transmission electron microscopy (TEM) [see Supporting Information (SI) Table 1 and SI Figure 1]. M60 CNTs were compared with fullerene nC60, which has no aggregating effect on platelets. Because both pristine M60 and nC60 are hydrophobic and insoluble in aqueous solutions, characterization of the dispersed nanomaterial agglomerate state in blood plasma is critical for evaluation of the interaction with platelets. Flow particle image analysis (SI Table 2 and SI Table 3) showed that both M60 and nC60 form agglomerates of a similar diameter, but vastly different shape, in plasma; the median particle sizes were 1.0 μm (10th—90th percentile = 0.4—2.9 μm), and 0.7 μm (10th—90th percentile = 0.4—1.5 μm) for M60 and nC60, respectively. The surface charges of both materials in plasma were close to zero, as demonstrated by zeta potential measurements (SI Table 4). The structures of the M60 and nC60 aggregates were determined by electron microscopy (EM); field-emission scanning electron microscopy (FESEM) and TEM showed numerous protuberances on the periphery of the M60 clusters, which were formed by a relatively long, dense net of highly tangled CNTs lacking a specific orientation. In contrast, nC60 particles were largely devoid of these surface features (SI Figure 1).

Platelet-CNP Interaction. Platelet morphology and intracellular structure after exposure to these nanomaterials were directly observed by TEM and FESEM. Figures 1a through 1e show the detailed topography of blood platelets exposed to different insults. The morphologies of nontreated platelets and platelets treated with nC60 are typical of the nonactivated state, that is, the platelets have a smooth surface and discoid shape.[9] The maximum platelet activation (positive control), as evidenced by strong aggregation, was achieved by treating platelets with thrombin receptor-activating peptide (TRAP).[10,11] M60 clearly induced similar platelet morphological changes, pseudopodia formation, membrane budding, and the release of membrane microparticles (MP), as shown in Figure 1e and Figure 1g.

An essential event during platelet activation is the increase in intracellular free calcium (Ca^{2+}).[12] In fact, we have shown[8] that CNT-induced platelet activation follows the influx of extracellular Ca^{2+}. The leading mechanism for Ca^{2+} entry in platelets is store-operated calcium entry (SOCE), a process controlled by the Ca^{2+} concentrations in the intracellular Ca^{2+} stores.[12] The DTS (similar to the endoplasmic reticulum in other cells) is the major source of Ca^{2+} in platelets,[13] and the depletion of Ca^{2+} from the DTS triggers the activation of SOCE channel in the plasma membrane to allow the influx of extracellular Ca^{2+}.[14] TEM and FESEM (Figure 1f and Figure 2a) show that M60 CNTs interact with the platelet plasma membrane (PM) and are translocated into the cytosol, as observed in other cell lines.[15,16] Although nC60 is also internalized (Figure 1h), it does not cause significant platelet
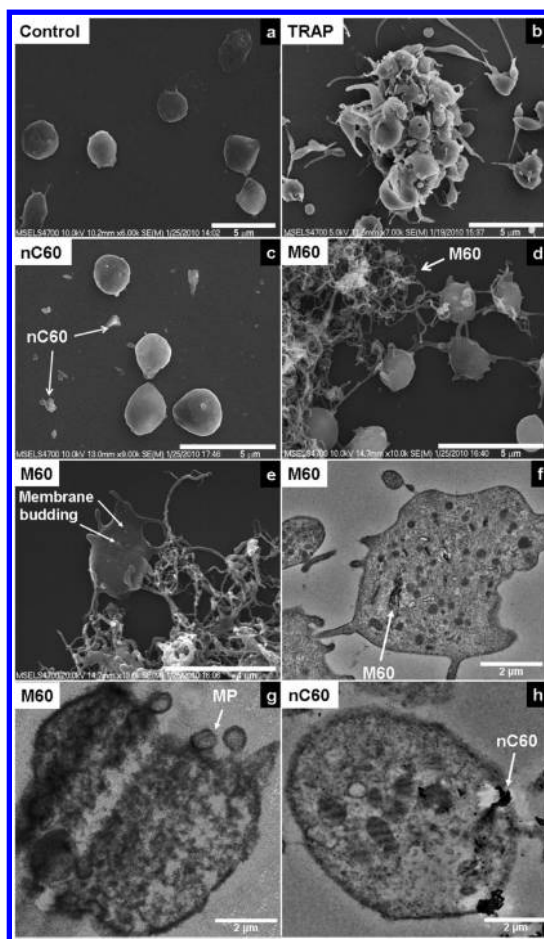
Figure 1. FESEM reveals morphological details of resting platelets (a) or platelets activated with TRAP (20 μmol/L; positive control) (b) or treated with 100 μg/mL of nC60 (c) or M60 (d). M60 induces membrane budding (e). TEM images of platelet cross sections showing the internalization of M60 (f) with pseudopodia formation, release of MP (g), and internalization of nC60 (h), which does not induce platelet activation. Platelets were incubated with TRAP or nanomaterials at 37 °C for 15 min under gentle agitation. The images are representative of at least three individual experiments with platelets from different donors.

activation. Having entered the platelets, M60 could induce mechanical injury (rupture) of DTS membranes or stimulate a local phase transition in the membrane phospholipid structure.[17] Both processes could lead to the depletion of Ca^{2+} from the DTS through leakage or passive efflux into the cytosol.[18] To test this hypothesis, TEM of the DTS was performed by labeling peroxidases with 3,3'-diaminobenzidine tetrahydrochloride hydrate (DAB)-osmium product;[19] Figure 2b shows M60 CNTs that are puncturing or in close proximity to the DTS membranes. Next, we measured the changes in the Ca^{2+} concentration in the platelet intracellular compartments using Fura-FF/AM, a fluorescent probe for Ca^{2+} that is used to measure Ca^{2+} from intracellular stores.[20,21] An increase in the fluorescence of Fura-FF/AM indicated the depletion of Ca^{2+} from stores, as demonstrated in Figure 2c. M60 and the sarco-endoplasmic reticulum calcium ATPase (SERCA) pump inhibitor
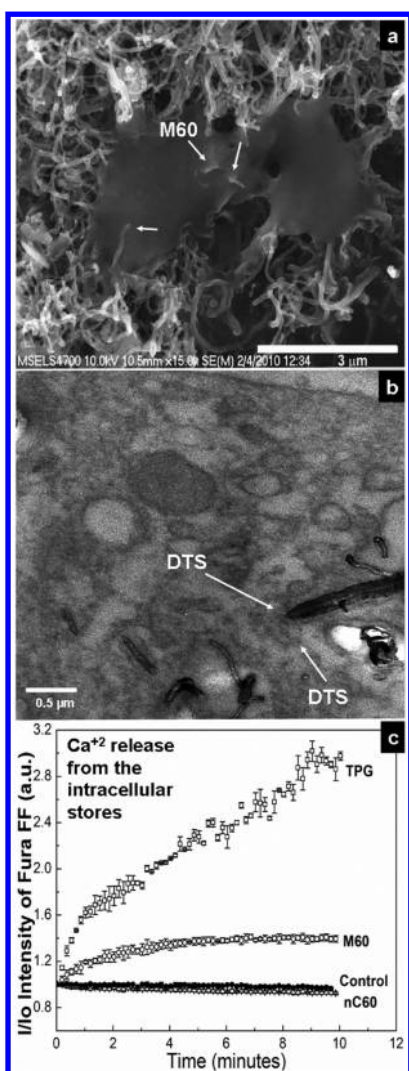
Figure 2. M60 penetrates the platelet plasma membrane and interacts with DTS to cause Ca^{2+} depletion. (a) FESEM image; platelet pseudopodia and CNTs are distinguished by the seeding of platelets without a conductive layer to increase the contrast between M60 and platelets. Peroxidases present in the DTS react with DAB (in the presence of 0.003% hydrogen peroxide), and the osmiophilic product is opaque to the electron beam and provides contrast to the DTS.[19] (b) TEM images of DAB-osmium-labeled platelet DTS. (c) Ca^{2+} release from the intracellular stores of permeabilized platelets (streptolysin 0.5 U/mL and 100 μmol/L EGTA added) measured by Fura-FF/AM. The images are representative of at least three individual experiments with platelets from different donors; error bars represent standard deviations.

thapsigargin (TPG) induce a marked decrease in Ca^{2+} in the DTS.[12] SERCA is responsible for refilling the Ca^{2+} stores, but in the presence of TPG, SERCA activity is blocked and the luminal Ca^{2+} content is passively effluxed to the cytoplasm. Under the same conditions, nC60 did not induce the depletion of Ca^{2+} from the stores, similar to the untreated control platelets.

SOCE activation induced by the CNTs. The depletion of Ca^{2+} from the DTS is usually not sufficient to activate platelets;[13] it is known that SOCE critically regulates platelet activation by allowing a much higher extracellular
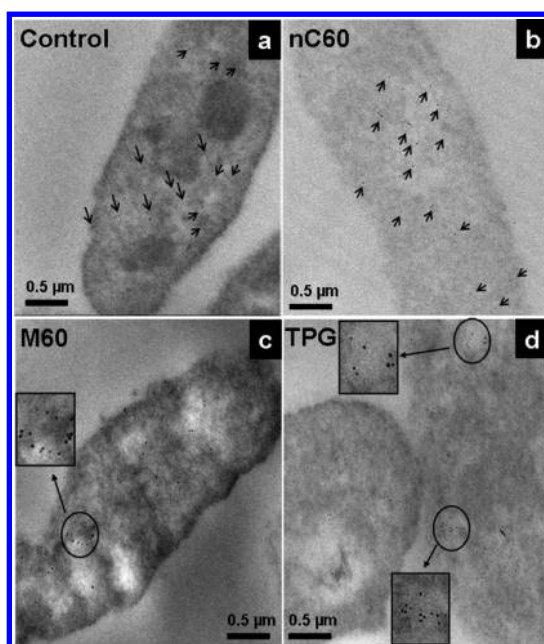

Figure 3. TEM images of 5-nm gold-conjugated anti-STIM1 (anti-GOK/STIM1)-labeled platelets. M60 (100 μg/mL) (c) and TPG (20 μmol/L) (d) induce STIM1 aggregation in platelets, while nC60 (100 μg/mL)-treated platelets (b) show a homogeneous distribution of STIM1 similar to that of the nontreated platelets (a). The images are representative of at least three individual experiments with platelets from different donors.

concentration of Ca^{2+} to enter, which leads to the cytoskeletal reorganization required for the platelet activation.[13]

Two major players in SOCE have been identified: the 4-transmembrane–spanning calcium release-activated channel moiety Orai1 and STIM1,[22] a Ca^{2+} sensor expressed predominantly in the DTS.[23] STIM1 molecules sense the depletion of Ca^{2+} from the DTS, oligomerize, translocate to junctions adjacent to the plasma membrane, and organize with Orai1 to form the elementary unit of SOCE activation.[22] To elucidate whether SOCE has a role in CNT-induced platelet activation, we evaluated the effect of M60 and nC60 on STIM1 aggregation by gold immunolabeling and laser scanning confocal microscopy (LSCM). Western blot analysis confirmed the target specificity of the anti-STIM1 antibody used for immunolabeling (SI Figure 2). Platelets were labeled with 5-nm gold- or Alexa 488-conjugated anti-STIM1 antibody and analyzed by TEM or LSCM, respectively. Figure 3 shows cross sections of platelets labeled with gold anti-STIM1; clusters of STIM1 were present in platelets exposed to TPG or M60, while STIM1 in platelets exposed to nC60 was homogeneously distributed in a manner similar to that of nonactivated control platelets.

LSCM measurements (Figure 4) visualized the clustering of STIM1 and its colocalization with Orai1 at discrete, tightly coupled DTS–PM junctions[22] after the treatment of platelets with TPG or M60 CNTs. Thus, our results demonstrate that SOCE plays a key role in CNT-induced platelet activation, as indicated in the proposed mechanism in Figure 5.
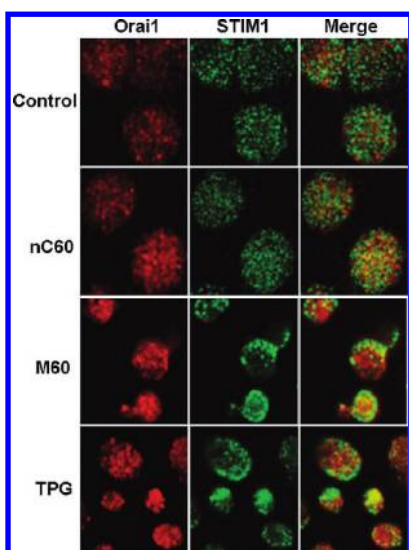
Figure 4. LSCM images of STIM1-(green) and Orai1-(red) labeled platelets. Platelets treated with nC60 show a STIM1 distribution similar to that of the nontreated samples. M60 (100 μg/mL) and TPG (6 μmol/L) induce STIM1 redistribution and colocalization with Orai1 in their discrete, tightly coupled DTS-PM junctions. Yellow in merged images signifies colocalization. The images are representative of at least three individual experiments with platelets from different donors.

Mechanism of Platelet Activation by CNTs. It is intuitive to consider that CNTs could injure the PM and cause extracellular Ca^{2+} entry. However, our previous work showed that CNT-induced platelet activation is minimized by Ca^{2+} entry inhibitors,[8] which implies that Ca^{2+} entry occurs through a regulated Ca^{2+} channel rather than through a damaged membrane. Moreover, our TEM and FESEM data did not reveal membrane breakage, suggesting that the membrane potentially self-seals around the nanotubes immediately after penetration, as previously reported for other cell types.[17,24,25] The interaction of CNTs with cell membranes is a subject of intense investigation,[26] but we still lack an in-depth understanding of the mechanism and biological consequences of such interactions. Recent studies have shown that CNTs can induce a membrane local phase transition,[17] which is known[18] to cause lipid bilayers to become leaky to Ca^{2+}. Interestingly, the cholesterol content in the DTS membrane is 5-fold lower[27,28] than that in the PM; the decreased cholesterol content was shown to decrease membrane resistance to structure "opening" and pore formation,[29] increase the susceptibility of membrane to injury, reduce the resealing rate,[30] and increase ionic transport.[31] Therefore, compared to
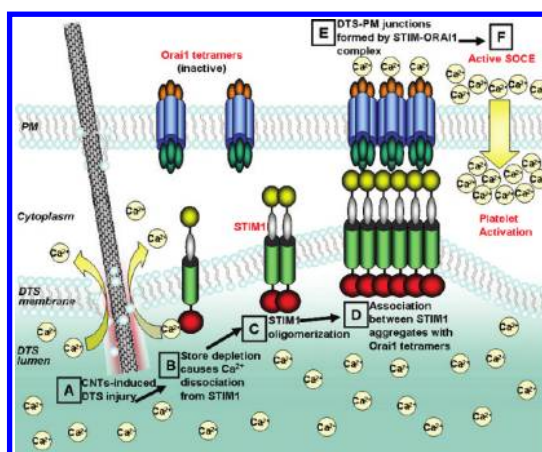
Figure 5. Mechanism of platelet activation by CNTs. (A) CNTs "nanopenetrate" platelets, causing injury to the DTS. (B) Ca^{2+} depletion from the DTS leads to Ca^{2+} dissociation from STIM1, causing (C) STIM1 oligomerization followed by the (D) diffusion, aggregation, and accumulation of STIM1 in DTS—plasma membrane junctions that (E) conformationally gates Orai1 to form a STIM1—Orai1 complex that (F) activates SOCE for Ca^{2+} influx.[22]

the PM, the DTS membrane seems to be more vulnerable to local phase transition and injury induced by CNTs, resulting in the increased passive permeability of Ca^{2+}. Compared to the effect of TPG, the M60-induced depletion of Ca^{2+} from stores is slower and less effective, as seen in Figure 2d, but sufficient to trigger STIM1 clustering and SOCE activation.

In summary, we elucidated the underlying molecular mechanisms for the platelet-activating[8] and potentially thrombogenic[3] effect of pristine MWCNTs. We demonstrated the ability of MWCNTs to nanopenetrate the platelet plasma membrane and interfere with Ca^{2+} homeostasis. MWCNTs caused no discernible plasma membrane damage possibly due to the ability of the lipid bilayer to self-sealing around the nanotubes. However, the interaction of MWCNTs with the DTS causes depletion of Ca^{2+} from the intracellular store. This process was accompanied with STIM1 clustering and its colocalization with Orai1, indicating the activation of SOCE. Thus, SOCE plays a pivotal role in the CNT-induced platelet activation. Understanding the nature of the interaction of CNTs with platelets will ultimately advance the development of general concepts for designing and testing carbon nanomaterials for optimal biocompatibility in blood. The challenge for the future is to investigate how the surface modifications of CNTs modulate these effects, which will allow more accurate risk assessment and increase the safety of these engineered nanomaterials.

METHODS

Materials. Multiwalled carbon nanotubes (MWCNTs; purity >95%) with outer diameters of 60−100 nm and lengths of 1−2 μm and fullerene (nC60; purity >99.9%) were purchased from SES Research. 3,3′-Diaminobenzidine tetrahydrochloride hydrate (DAB), EGTA, apyrase, prostaglandin E1, NaCl, HEPES-KOH, KCl, $MgCl_2$ and streptolysin were purchased from Sigma-Aldrich. Sodium cacodylate, Spur resin, glutaraldehyde, paraformaldehyde and osmium tetroxide were purchased from Electron Microscopy Science. Mouse Anti-GOK/STIM1 and anti-Orai1 antibodies were

purchased from BD Bioscience and ProSci, respectively. STIM1 peptide and anti-STIM1 were purchased from ProSci. Immunogold-conjugates (5 nm) goat antimouse IgG, Alexa Fluor 633-conjugated donkey antigoat IgG, Alexa Fluor 488-conjugated goat antimouse IgG, Image-iT FX signal enhancer, Fura-FF/AM, pluronic F-127, thapsigargin (TG) and F(ab')2 fragment of alkaline phosphatase-conjugated goat antirabbit IgG were purchased from Invitrogen. Thrombin receptor-activating peptide SFLLRN (TRAP-6) was from AnaSpec Inc. Alkaline phosphatase-conjugated AffiniPure F(ab')s fragment donkey antimouse IgG was from Jackson ImmunoResearch. All other reagents were of analytical grade and purchased from Sigma-Aldrich.

Platelet-CNP interaction. Platelet-rich plasma (PRP) was prepared from the blood of healthy donors (ACD anticoagulated, Department of Transfusion Medicine, Clinical Center, NIH, Bethesda, MD). A 50 mL portion of whole blood was centrifuged at 150g for 10 min at room temperature (RT), and the PRP was collected. The sediment was then centrifuged at 1000g for 15 min to obtain the platelet-poor plasma (PPP). The PRP platelet count was performed using an ABX Pentra 60, Horiba ABX, Inc., Irvine, CA. A stock solution was prepared by diluting the PRP with PPP to 250 × 10^3 platelets/μL, after which the platelet solution was incubated at 37 °C for 30 min. As described previously,[8] the interaction of nC60 and M60 CNTs with human blood platelets was analyzed by mixing 450 μL platelet stock solution with 50 μL nanoparticle suspension (freshly prepared solution, 1 mg/mL), TRAP or TG (final concentrations were 20 μmol/L and 6 μmol/L, respectively) and incubating at 37 °C for 15 min under gentle agitation. The ultrastructural analysis of the CNP-platelet interaction was performed by FESEM and TEM. For FESEM, platelets were fixed with 4% paraformaldehyde (PA) for 30 min, carefully deposited onto clean glass coverslips by cytospin, washed twice with PBS, fixed with 2% glutaraldehyde (GTA), washed extensively with cacodylate buffer, dehydrated in an ethanol series, washed with tetramethylsilane and dried at RT under vacuum. Some samples were sputter-coated with a thin film of gold at 13.3 Pa and 45 mA for 90 s. For the TEM, platelets were fixed in 4% PA and 1% GTA for 1 h, postfixed with 4% osmium tetroxide (OsO$_4$) solution in cacodylate buffer, dehydrated in an ethanol series, embedded with Spur and polymerized for 2 days at 65 °C. Ultrathin sections (aproximately 60 nm) were cut on a Leica ultramicrotome and collected onto 600 mesh copper grids.

Dense Tubular System Visualization by Peroxidase Labeling with DAB.[19] Platelets were fixed with 0.1% GTA in PBS for 15 min, washed twice with PBS to remove the excess plasma proteins, fixed with 2.5% PA and 0.5% GTA for 30 min, washed extensively with 0.05 mol/L Tris buffer and incubated overnight with DAB solution (2.5 mg/mL in 0.05 mol/L Tris buffer) at 4 °C. On the following day, the DAB solution was replaced with freshly prepared DAB solution containing 0.003% hydrogen peroxide and incubated for 2 h at RT. The platelets were then extensively washed with cacodylate buffer, postfixed with 4% OsO$_4$ for 1 h at RT in the dark, dehydrated in an ethanol series, embedded in Spur and sectioned using a microtome for TEM.

STIM1 Gold Immunolabeling. SDS-PAGE and Western blot analysis of STIM1 from platelets to confirm the target specificity of the anti-STIM1 antibody used for immunolabeling was performed as previously described.[32] STIM1 in platelets was labeled for TEM as follows: after platelets were incubated with CNPs or TPG, as described above, samples were fixed with 1% PA for 15 min, washed three times with PBS, and permeabilized with 0.1% Triton X-100 for 15 min. After extensive washes with PBS, the platelets were blocked with Image-iT FX signal enhancer for 30 min. The platelets were then incubated with 150 μL of mouse anti-GOK/STIM1 antibody (10 μg/mL) for 2 h, washed 4 times with PBS for 5 min each time, and incubated with 5-nm immunogold-conjugated goat antimouse IgG (150 μL, 10 μg/mL) for 2 h at RT. After five washes with PBS for 5 min each, the samples were fixed with 2.0% PA and 2.5% GTA for 30 min at RT to avoid artifacts during the embedding process required for the TEM, as described above. All of the above steps were performed at RT.

Confocal Microscopy. STIM1 and Orai1 in platelets were labeled for laser scanning confocal microscopy (LSCM) using the protocol described above, except the immunogold conjugate was replaced with Alexa Fluor 488-conjugated goat antimouse IgG to detect STIM1 and Alexa Fluor 633-conjugated donkey antigoat IgG to detect Orai1. After the incubation with the antibodies, the samples were extensively washed with PBS. The platelets were then deposited onto a clean glass slide by cytospin, mounted with VectaShield and imaged with a Zeiss 710 LSM 710 NLO with a Plan Apochromat 100x/1.40 oil objective. Once adjusted, the laser configuration and pinhole aperture were kept the same for all samples analyzed. MatLab and Image J software were used for image deconvolution.

Intracellular Ca^{2+} Measurement. Qualitative analysis of the Ca^{2+} content in platelets was performed as per Rosado et al.[21] with some modifications. The PRP (10^8 cells/mL) was incubated at 37 °C with 5 μmol/L Fura-FF/AM and pluronic F-127 (0.025%) for 45 min, after which 1 μM prostaglandin E1 was added. After 10 min, the cells were collected by centrifugation at 350g for 10 min and resuspended in a modified intracellular solution containing 20 mmol/L NaCl, 10 mmol/L HEPES-KOH, 120 mmol/L KCl, and 1.13 mmol/L MgCl$_2$, at pH 7.2, and supplemented with 40 μg/mL apyrase; EGTA (100 μmol/L) was then added 10 min before the experiment started. Cell membranes were permeabilized, allowing cytosolic Ca^{2+} to be chelated, by mixing 225 μL of Fura-FF/AM-loaded platelets placed in a 96-well plate with 0.5 U/mL streptolysin. After 1 min, 25 μL M60, nC60 or TPG (6 μmol/L) solution was added to begin the experiment. Changes in the Ca^{2+} content in platelet stores were monitored by measuring the excitation at 380 nm and emission at 510 nm.

REFERENCES AND NOTES

1. Owens, A. P., 3rd; Mackman, N. Tissue Factor and Thrombosis: The Clot Starts Here. *Thromb. Haemost.* **2010**, *104*, 432–439.

2. Ryman-Rasmussen, J. P.; Cesta, M. F.; Brody, A. R.; Shipley-Phillips, J. K.; Everitt, J. I.; Tewksbury, E. W.; Moss, O. R.; Wong, B. A.; Dodd, D. E.; Andersen, M. E.; Bonner, J. C. Inhaled Carbon Nanotubes Reach the Subpleural Tissue in Mice. *Nat. Nanotechnol.* **2009**, *4*, 747–751.

3. Radomski, A.; Jurasz, P.; Alonso-Escolano, D.; Drews, M.; Morandi, M.; Malinski, T.; Radomski, M. W. Nanoparticle-Induced Platelet Aggregation and Vascular Thrombosis. *Br. J. Pharmacol.* **2005**, *146*, 882–893.

4. Bihari, P.; Holzer, M.; Praetner, M.; Fent, J.; Lerchenberger, M.; Reichel, C. A.; Rehberg, M.; Lakatos, S.; Krombach, F. Single-Walled Carbon Nanotubes Activate Platelets and Accelerate Thrombus Formation in the Microcirculation. *Toxicology* **2010**, *269*, 148–154.

5. Kostarelos, K.; Bianco, A.; Prato, M. Promises, Facts and Challenges for Carbon Nanotubes in Imaging and Therapeutics. *Nat. Nanotechnol.* **2009**, *4*, 627–633.

6. Evelyn, A.; Mannick, S.; Sermon, P. A. Unusual Carbon-Based Nanofibers and Chains Among Diesel-Emitted Particles. *Nano Lett.* **2003**, *3*, 63–64.

7. Kam, N. W. S.; O'Connell, M.; Wisdom, J. A.; Dai, H. J. Carbon Nanotubes as Multifunctional Biological Transporters and Near-Infrared Agents for Selective Cancer Cell Destruction. *Proc. Natl. Acad. Sci. U.S.A.* **2005**, *102*, 11600–11605.

8. Semberova, J.; De Paoli Lacerda, S. H.; Simakova, O.; Holada, K.; Gelderman, M. P.; Simak, J. Carbon Nanotubes Activate Blood Platelets by Inducing Extracellular Ca^{2+} Influx Sensitive to Calcium Entry Inhibitors. *Nano Lett.* **2009**, *9*, 3312–3317.

9. Jackson, S. P. The Growing Complexity of Platelet Aggregation. *Blood* **2007**, *109*, 5087–5095.

10. Simak, J.; Holada, K.; Janota, J.; Stranak, Z. Surface Expression of Major Membrane Glycoproteins on Resting and TRAP-Activated Neonatal Platelets. *Pediatr. Res.* **1999**, *46*, 445–449.

11. Furman, M. I.; Liu, L. B.; Benoit, S. E.; Becker, R. C.; Barnard, M. R.; Michelson, A. D. The Cleaved Peptide of the Thrombin Receptor Is a Strong Platelet Agonist. *Proc. Natl. Acad. Sci. U.S.A.* **1998**, *95*, 3082–3087.

12. Redondo, P. C.; Salido, G. M.; Pariente, J. A.; Sage, S. O.; Rosado, J. A. SERCA2b and 3 Play a Regulatory Role in Store-Operated Calcium Entry in Human Platelets. *Cell Sig.* **2008**, *20*, 337–346.

13. Jardin, I.; Lopez, J. J.; Pariente, J. A.; Salido, G. M.; Rosado, J. A. Intracellular Calcium Release from Human Platelets: Different Messengers for Multiple Stores. *Trends Cardiovasc. Med.* **2008**, *18*, 57–61.

14. Varga-Szabo, D.; Braun, A.; Nieswandt, B. Calcium Signaling in Platelets. *J. Thromb. Haemost.* **2009**, *7*, 1057–1066.

15. Becker, M. L.; Fagan, J. A.; Gallant, N. D.; Bauer, B. J.; Bajpai, V.; Hobbie, E. K.; Lacerda, S. H.; Migler, K. B.; Jakupciak, J. P. Length-Dependent Uptake of DNA-Wrapped Single-Walled Carbon Nanotubes. *Adv. Mater.* **2007**, *19*, 939–943.

16. Porter, A. E.; Gass, M.; Muller, K.; Skepper, J. N.; Midgley, P. A.; Welland, M. Direct Imaging of Single-Walled Carbon Nanotubes in Cells. *Nat. Nanotechnol.* **2007**, *2*, 713–717.

17. Wallace, E. J.; Sansom, M. S. Blocking of Carbon Nanotube Based Nanoinjectors by Lipids: A Simulation Study. *Nano Lett.* **2008**, *8*, 2751–2756.

18. Tsvetkova, N. M.; Crowe, J. H.; Walker, N. J.; Crowe, L. M.; Oliver, A. E.; Wolkers, W. F.; Tablin, F. Physical Properties of Membrane Fractions Isolated from Human Platelets: Implications for Chilling Induced Platelet Activation. *Mol. Membr. Biol.* **1999**, *16*, 265–272.

19. White, J. G. Electron Microscopy Methods for Studying Platelet Structure and Function. *Methods Mol. Biol.* **2004**, *272*, 47–63.

20. Wokosin, D. L.; Loughrey, C. M.; Smith, G. L. Characterization of a Range of Fura-Dyes with Two-Photon Excitation. *Biophys. J.* **2004**, *86*, 1726–1738.

21. Lopez, J. J.; Redondo, P. C.; Salido, G. M.; Pariente, J. A.; Rosado, J. A. Two Distinct Ca^{2+} Compartments Show Differential Sensitivity to Thrombin, ADP and Vasopressin in Human Platelets. *Cell Signal* **2006**, *18*, 373–381.

22. Deng, X.; Wang, Y.; Zhou, Y.; Soboloff, J.; Gill, D. L. STIM and Orai: Dynamic Intermembrane Coupling to Control Cellular Calcium Signals. *J. Biol. Chem.* **2009**, *284*, 22501–22505.

23. Wei, A. H.; Schoenwaelder, S. M.; Andrews, R. K.; Jackson, S. P. New Insights into the Haemostatic Function of Platelets. *Br. J. Haemat.* **2009**, *147*, 415–430.

24. Pogodin, S.; Slater, N. K.; Baulin, V. A. Surface Patterning of Carbon Nanotubes Can Enhance Their Penetration Through a Phospholipid Bilayer. *ACS Nano* **2011**, *5*, 1141–1146.

25. Chen, X.; Kis, A.; Zettl, A.; Bertozzi, C. R. A Cell Nanoinjector Based on Carbon Nanotubes. *Proc. Natl. Acad. Sci. U.S.A.* **2007**, *104*, 8218–8222.

26. Yang, K.; Ma, Y. Q. Computer Simulation of the Translocation of Nanoparticles with Different Shapes across a Lipid Bilayer. *Nat. Nanotechnol.* **2010**, *5*, 579–583.

27. Fauvel, J.; Chap, H.; Roques, V.; Levy-Toledano, S.; Douste-Blazy, L. Biochemical Characterization of Plasma Membranes and Intracellular Membranes Isolated from Human Platelets Using Percoll Gradients. *Biochim. Biophys. Acta* **1986**, *856*, 155–164.

28. Menashi, S.; Weintroub, H.; Crawford, N. Characterization of Human Platelet Surface and Intracellular Membranes Isolated by Free Flow Electrophoresis. *J. Biol. Chem.* **1981**, *256*, 4095–4101.

29. Koronkiewicz, S.; Kalinowski, S. Influence of Cholesterol on Electroporation of Bilayer Lipid Membranes: Chronopotentiometric Studies. *Biochim. Biophys. Acta* **2004**, *1661*, 196–203.

30. Vlahakis, N. E.; Schroeder, M. A.; Pagano, R. E.; Hubmayr, R. D. Role of Deformation-Induced Lipid Trafficking in the Prevention of Plasma Membrane Stress Failure. *Am. J. Respir. Crit. Care Med.* **2002**, *166*, 1282–1289.

31. Corvera, E.; Mouritsen, O. G.; Singer, M. A.; Zuckermann, M. J. The Permeability and the Effect of Acyl-Chain Length for Phospholipid Bilayers Containing Cholesterol: Theory and Experiment. *Biochim. Biophys. Acta* **1992**, *1107*, 261–270.

32. Brouckova, A.; Holada, K. Cellular Prion Protein in Blood Platelets Associates with Both Lipid Rafts and the Cytoskeleton. *Thromb. Haemost.* **2009**, *102*, 966–974.